JOURNAL OF MATERIALS SCIENCE **39** (2004) 3047– 3055

The thermo-mechanical behaviour of Cu-Cr *in-situ* composite

K. L. LEE
Department of Engineering, University of Leicester, University Road, Leicester LE1 7RH, UK
E-mail: KoKLoong1@hotmail.com

The mechanical response of *in-situ* copper-chromium composite was modelled using a deformation mechanism map approach. The stresses in each phase were predicted as a function of temperature and strain rate. From this the ratio of phase stresses, and hence the degree of load transfer, was obtained. The extent of load transfer and the predicted deformation modes of the two phases were then related to the expected failure mechanisms of the composite. Three modes of composite failure were predicted. Copper-chromium *in-situ* composites, and pure copper, were produced by a casting and swaging route. The mechanical properties were then characterised experimentally by tensile testing. Mechanical tests confirmed that the composite showed significantly higher strength than the unreinforced material. The observed failure modes of the composite were compared with the predictions.

1. Introduction

The current demand is for conductive materials with mechanical properties which are superior to those exhibited by monolithic Cu. *In-situ* composites provide a solution to this problem by the introduction of a stiffer reinforcement phase which bears a significant proportion of the applied load. This allows the material to carry higher loads than unreinforced Cu. At the same time, there are two obvious advantages in using *in-situ* composites. Firstly, conventional processing techniques, such as casting, can be employed, resulting in lower production costs compared with conventional composites, and secondly, the reinforcement phase can contribute to the conductivity, unlike traditional ceramic reinforcements. It has been established that metals with bcc structure are particularly suited to reinforcing an fcc metal matrix, because when subjected to high degrees of deformation, they elongate preferentially, resulting in a fine ribbon-like morphology [1–8].

To date, considerable work has been directed towards the initial development of high thermal and electrical conductivity materials with high strength [8]. However, industry still faces problems in using these materials for electronics and aerospace applications. The main focus of the current studies has been on production and optimisation of the as-fabricated properties [7]. For instance, considerable work has been done on Cu-based alloys prepared by rapid solidification and mechanically alloyed metal composites [9], both to optimise the mechanical and thermal processing parameters, and to characterise the initial microstructure. In Japan, considerable research has been done on cast/drawn Cu-Cr composites which has concentrated on optimising the tensile strength and conductivity in terms of processing variables and subsequent ageing behaviour [10, 11].

However, important questions remain unanswered. The in-service response of these materials has not been investigated. Without this knowledge they cannot be fully and safely exploited. The effect of load transfer, thermo-mechanical loading and the ensuing damage cannot be ignored. Damage will have a deleterious effect on both the conductivity of the composite, and its mechanical response. Moreover, their properties cannot be well understood without considering them in terms of composite theory; an approach which has not previously been examined.

In a conventional MMC, elastic and/or plastic deformation in the matrix causes a misfit between the matrix and the reinforcement, which in turn results in load transfer to the reinforcement. However, Cu-Cr *in-situ* composites differ fundamentally from conventional composites in that both phases are able to deform plastically. Therefore, the degree of load transfer is governed by the relative extent of deformation in each phase, and this in turn depends upon the dominant deformation mechanism operating in each phase at a given temperature. In order for the composite's deformation and subsequent failure mechanisms to be fully understood, it is necessary to quantify the extent of load transfer as a function of temperature and strain rate.

In this research, the deformation rate of each phase is predicted using model-based strain-rate equations

Current address: Department of Semis and Rods (Technical), Corus Construction & Industrial, PO Box 1, Brigg Road, Scunthorpe, North Lincolnshire, DN16 1BP, UK.

as outlined by Frost and Ashby [12]. From this the overall composite deformation rate is derived and is presented in a deformation map form. This is used to obtain information regarding the extent of load transfer in the composite as a function of testing temperature and strain rate, and hence regimes of failure mechanism. Predictions are then compared with experimental results.

2. Experimental procedure

2.1. Materials

The Cu-10 vol% Cr *in-situ* composite used in this study was produced by vacuum casting at 1870 K by Essex Metallurgical Limited. The final ingot was approximately 14.5 mm in diameter. It was then hot forged at 1170 K and swaged at room temperature into 3 mm diameter rod. Deformation reduction can be expressed in terms of true strain η by:

$$\eta = \ln\left(\frac{A_i}{A_f}\right) \tag{1}$$

where A_i is the initial cross sectional area of the specimen, and A_f is the final cross sectional area after deformation. This true strain must be greater than around 3 (equivalent to a reduction in area of approximately 95%) to achieve any strengthening effect in the composite. In the 3 mm rod, the deformation strain η was 3.15 which was approximately 95.6% reduction in area.

2.2. Material characterisation

The microhardness of the Cu and Cr phases in the composite was measured on a Mitutoyo MVK-G1 microhardness testing machine. The testing was performed under a 98 N load for 10 s on a polished longitudinal section of the composites. The final results are the average of 10 indentations on each specimen. A total of 3 specimens were used.

Tensile tests were carried out on a Hounsfield machine at temperatures ranging from −70 to 600°C under displacement control at a rate of 1 mm min^{-1}, with the Cr fibres parallel to the loading direction. The axial strain was monitored by using a video extensometer (ME-46 Full Image Video extensometer). For tests performed at elevated temperatures, a 3 kW heating element was used, with the specimens and attached equipment given 30 min at elevated temperature before testing began. To ensure a uniform heat distribution on the specimen, 4 ceramic heaters were arranged to form a circle around it. No load was applied to the specimen during heating, and the specimen was removed immediately after testing to minimise any creep effects. Cryogenic tests were performed by spraying liquid nitrogen directly onto the specimen. The supply of liquid nitrogen to the specimen was automatically cut-off when the desired temperature (–70°C) was achieved as measured by a thermocouple in contact with the sample. The temperature accuracy of this method was about ±5°C.

After testing, specimens were sectioned and the microstructure examined using optical and SEM techniques. Initially, specimens were mechanically polished and etched with dilute chromic acid to reveal the Cu grain structure. After this, the specimens were deep etched using 40% HNO_3, prior to examination in the SEM, in order to reveal microstructural damage.

3. Results and discussion

3.1. Microstructural evolution

In the original cast state, the Cr was in a dendritic form as shown in Fig. 1. The dimensional of dendritic Cr (including dendritic arms) varies from 20–100 μm. Because the difference in density is relatively slight (ρ_{Cu} = 8.93 gcm^{-3} and ρ_{Cr} = 7.14 gcm^{-3}) gravitational segregation of the primary dendrites during casting is not a major concern. During subsequent deformation, the Cr dendrites (the finer the dendrite size,

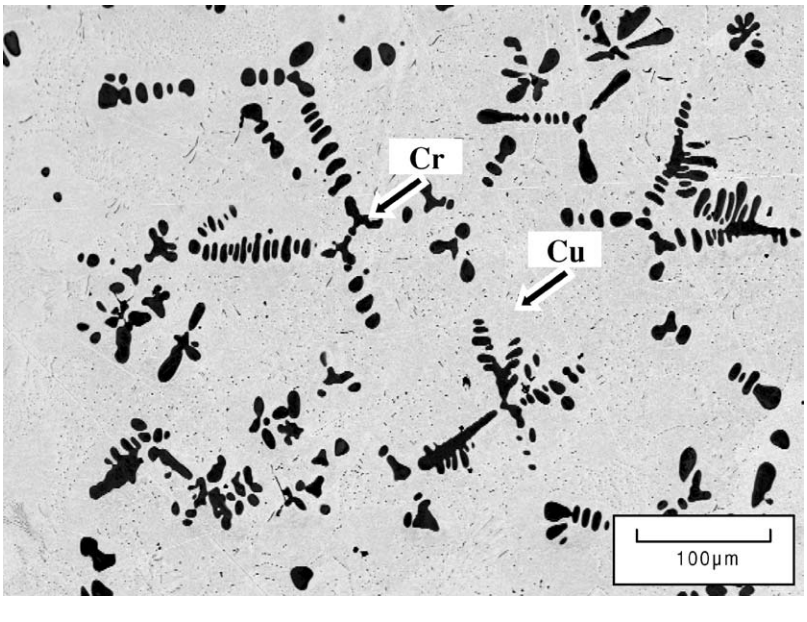

Figure 1 SEM image of the as-cast composite, the Cu matrix having being selectively etched away.

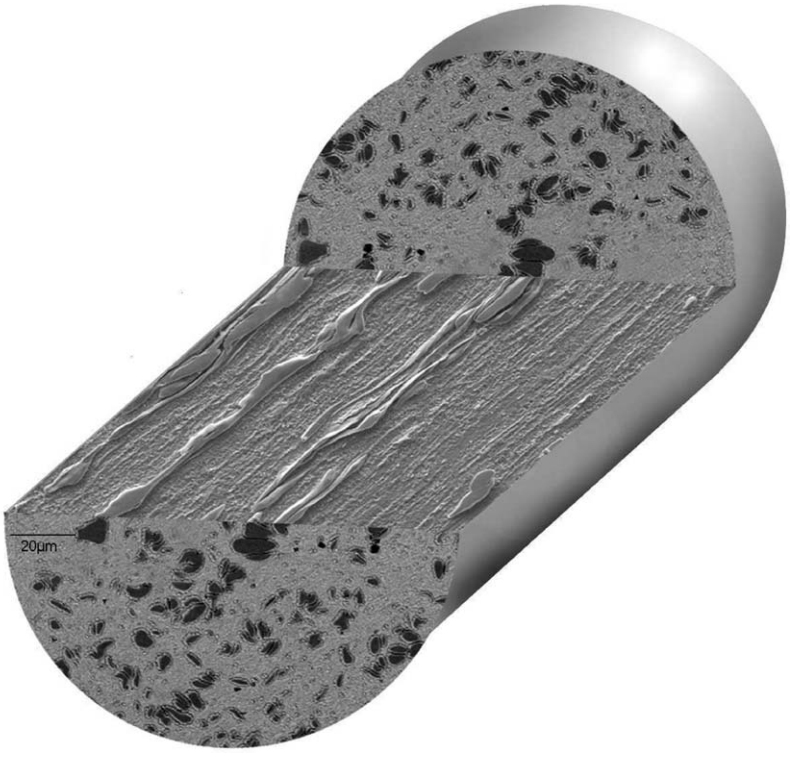

Figure 2 Three-dimensional representation of the microstructure from backscattered SEM micrographs after deformation to $\eta = 3.15$. The Cr fibres (darker phase) lie parallel to the specimen rod (swaging) axis.

the higher the flow stress subsequent to deformation) elongated into fibres parallel to the swaging axis as shown in Fig. 2. It can be seen that after deformation, the original morphologies of dendritic Cr and equiaxed Cr could not be distinguished. The mean thickness of the Cr fibres was 2 μm with an aspect ratio of 25:1 (dimension parallel to the rod axis: dimension perpendicular to the rod axis) as measured from 10 SEM micrographs. A few fibres with a thickness of about 10 μm and an aspect ratio of 10 were also found in this composite. The good interfacial bonding between Cu and Cr makes the large deformation possible without any interfacial failure, which is one of the advantages of *in-situ* composites.

3.2. Mechanical properties

3.2.1. Hardness

Table I shows the hardness of the Cu and Cr phases in the as-cast and as-swaged conditions. The hardness of the Cu phase increases significantly from 65 to 110 in the average Vickers hardness number (VHN) as the swaging strain increases from 0 to 3.15. This shows the dramatic work hardening of the Cu phase. The hardness of the Cr phase also increases from the as-cast to the as-swaged condition, but the change is much more modest than that of the Cu phase. A similar trend was also reported for Cu-15vol% Cr-0.2Ti composite [13]. With a further increase in drawing strain, the hardness of the Cu phase continues to increase, but the rate of increase becomes lower [13].

TABLE I Hardness of the Cu and Cr phases in the as-cast and as-swaged conditions

	Vickers hardness (VHN)	
Phases	As-cast	As-swaged
Cu	65 (±5)	110 (±8)
Cr	185 (±7)	202 (±6)

3.2.2. Tensile response

The stress-strain plots obtained at nine testing temperatures are shown in Fig. 3. These plots show that the presence of the Cr fibres increases the room temperature yield strength of the material by 77% and the ultimate tensile strength of the material by 43% compared to those of pure Cu. The ductility of the material is relatively low at all temperatures and decreases as the temperature decreases. It is well known that the ductility of the Cu-based composites decreases with increasing drawing strain [13]. This decrease in ductility with increasing drawing strain is caused by the work hardening of the Cu matrix and decrease in the inter-fibre spacing.

As expected the addition of Cr results in a significant increase in the Young's modulus and load bearing capacity of the composite with a corresponding loss in ductility. The Young's modulus of the composite may be calculated using the "Rule of Mixtures" (ROM) relationship assuming the isostrain loading condition. Substituting $E_f = 280$ GPa, $E_m = 135$ GPa, and $V_f = 0.1$ into ($E_{composite} = E_f V_f + E_m(1 - V_f)$) gives a composite modulus of 149.5 GPa. The Young's modulus predicted assuming isostrain loading condition ($E_{composite} = E_f V_f + E_m(1 - V_f)$) is greater than that of isostress loading condition ($E_{composite} = E_f E_m/(V_f E_m + (1 - V_f)E_f)$. Here, E_f and E_m are the Young's modulus of fibre and matrix

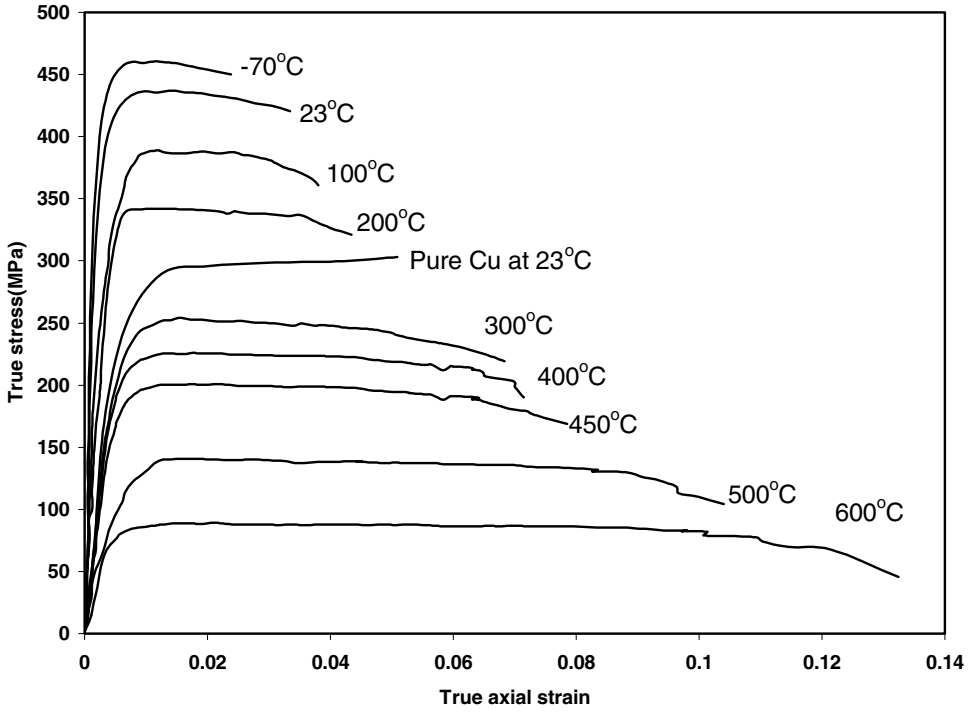

Figure 3 Stress/strain response for similarly processed unreinforced copper Cu (RT) and Cu-10 vol% Cr composite tested from –70 to 600°C.

respectively, and V_f is the fibre volume fraction. Substituting $E_f = 280$ GPa, $E_m = 135$ GPa, and $V_f = 0.1$ into this expression gives a composite modulus of 149.5 GPa for isostrain loading condition and 142 GPa for isostress loading condition.

Since the aspect ratio of Cr fibres is fairly high and fibres are aligned parallel to the loading axis, the real modulus should be close to that (149.5 GPa) for isostrain loading condition. The slope of the elastic region in Fig. 3 for the composite tested at room temperature is 142 GPa, which is close to the calculated ROM value. The good agreement between the experimental modulus and that of isostress loading condition does not necessarily mean that Cr fibres and Cu matrix are loaded in series since the predicted values are within the range of experimental error. The experimental modulus from mechanical testing is likely to be a little lower than the real modulus possibility for early micro-yielding. The composite failure mechanisms are discussed in the following section.

3.2.3. Prediction of composite response

In order to quantify the extent of load transfer occurring in the composite, an Ashby deformation mechanism map approach was used [14]. Data for the deformation of Cu and Cr was taken from Frost and Ashby [12]. In this method, the strain rate due to various microstructural deformation processes, (for example diffusional creep, obstacle controlled glide etc.) is calculated for different values of applied stress and temperature. From this, the overall strain rate and the dominant mechanism operating under particular conditions can be identified. The strain rate equations used are given in the Appendix.

Initially, deformation maps were derived for the Cu and Cr phases under uniaxial applied stress. From these, the overall composite deformation rate was obtained using a standard rule of mixtures. This approach is appropriate for determining the overall deformation response of the class of composite microstructures shown in Fig. 2. A plot showing the σ_{Cr}:σ_{Cu} stress ratio was then obtained using the calculated phase stresses. This gave a measure of the extent to which load is transferred to the reinforcement as a function of strain rate and temperature.

The deformation mechanism map for Cu-10 vol% Cr *in-situ* composite is shown in Fig. 4. On comparison with deformation maps of the individual phases, it is found that the response is dominated by the deformation of the Cu, although the increasing intrinsic lattice resistance of the Cr at low temperatures is responsible for a greater temperature sensitivity. The composite behaviour can be divided into five regimes, according to the mechanisms of deformation which dominates within each phase (as defined in Fig. 4). The overall trends are described as follows: at low temperatures, the Cr is brittle in a plastic Cu matrix, hence the two dominating mechanisms are lattice resistance controlled glide in the Cr and obstacle controlled glide in the Cu; as the temperature is increased, so both phases are able to deform plastically, and obstacle controlled glide dominates the behaviour in both Cu and Cr; at higher temperatures creep becomes the dominant deformation mechanism, first for the Cu and then for the Cr.

The material response will depend critically on the efficiency with which load is transferred to the reinforcement during deformation. This, in turn, depends on the misfit generated between the two phases. The composite deformation mechanism map (Fig. 4) confirms that the ease with which each phase deforms, and hence the degree of misfit and load transfer, is highly sensitive to both the temperature and the strain rate.

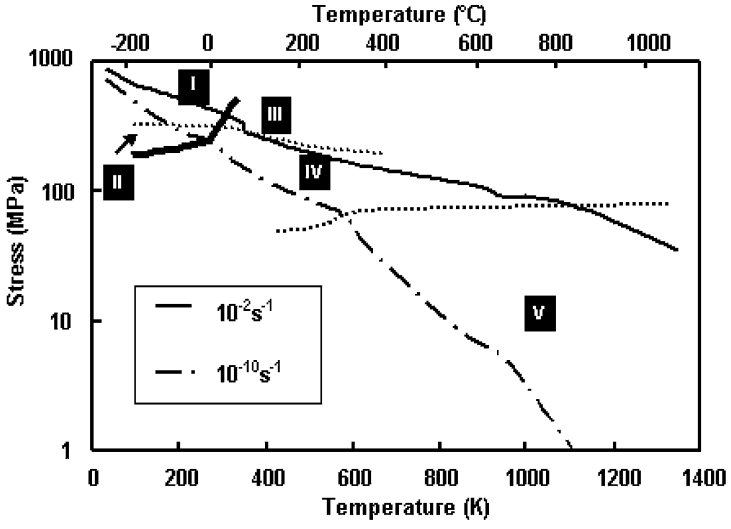

I - Obstacle Controlled Glide Cu - Lattice Resistance Controlled Glide Cr

II - Obstacle controlled glide Cu - Obstacle controlled glide Cr

III - Creep Cu - Lattice Resistance Controlled Glide Cr

IV - Creep Cu - Obstacle Controlled Glide Cr

V - Creep Cu - Creep Cr

Figure 4 Deformation mechanism map for Cu-10 vol% Cr. The regimes I to V indicate the conditions under which certain deformation processes dominate in each of the two phases.

This is expected to have significant consequences on the mechanical performance and failure mechanisms.

The ratio of Cr stress to Cu stress as a function of strain rate and temperature is presented in Fig. 5. It can be seen that the behaviour of the composite, in terms of degree of load transfer, falls into three regimes. Around room temperature, the ratio of stress in the Cr to that in the Cu is approximately one. Therefore, at this temperature both phases are deforming by similar extents, and consequently no misfit is generated between the two phases. This means that the composite behaviour is essentially that of a two-phase alloy, with no appreciable load transfer occurring. This was confirmed by neutron diffraction studies, which showed that during tensile deformation at room temperature, the Cr was not preferentially loaded [2]. At low temperatures, the lattice resistance of the bcc Cr increases sharply, and therefore the Cr begins to behave more like the rigid reinforcement in a conventional composite. The Cu can still deform plastically, and therefore significant misfit

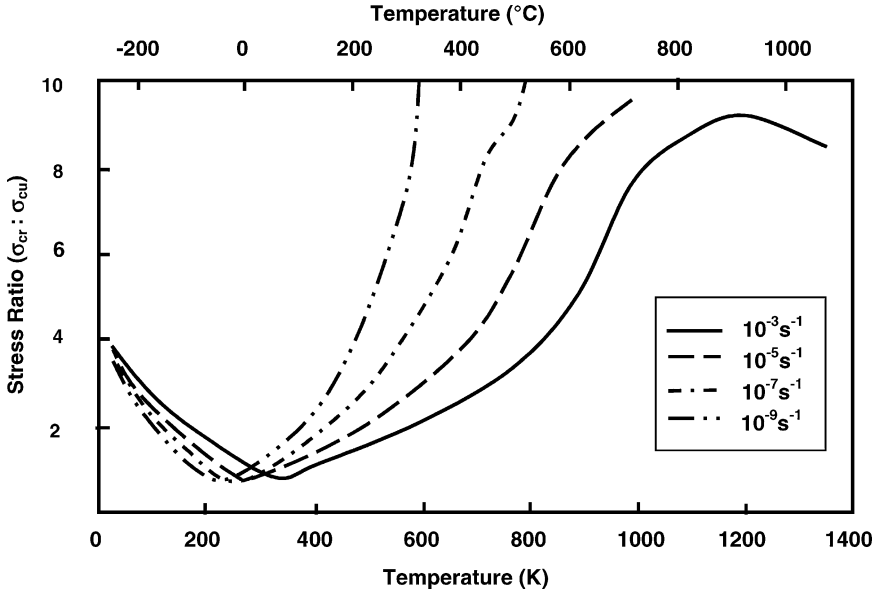

Figure 5 Ratio of stress in the Cr and Cu phases, as a function of temperature at different strain rates. Note that around room temperature, the ratio is ∼1, which implies that load transfer is negligible under these conditions.

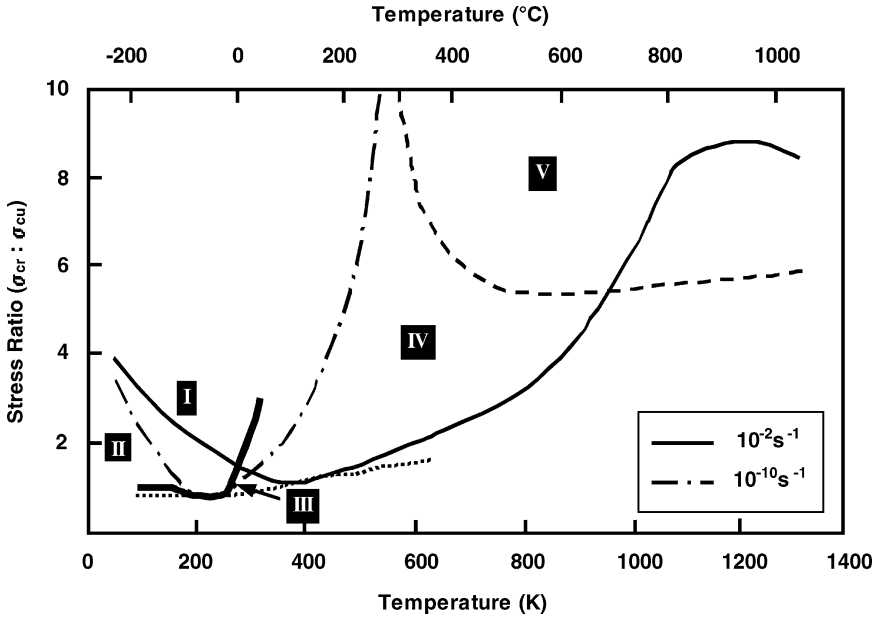

Figure 6 Stress ratio plot showing regimes of dominant deformation mechanism.

is generated during deformation giving rise to effective loading of the Cr reinforcement phase. At elevated temperatures, creep processes become significant in the Cu, leading to much easier deformation in this phase. As a result of this, significant misfit is generated between the two phases during deformation, and the Cr reinforcement is loaded preferentially. This shows that the Cr is effective as a reinforcement only when its deformation behaviour differs significantly from that of the Cu [15].

It can also be seen from Fig. 5 that the deformation rate has a significant influence on the composite behaviour. As the strain rate decreases, so the response curve shifts to lower temperatures. This is to be expected, since time dependent deformation mechanisms will be more significant at lower strain rates. Therefore, under a low strain rate there will be an increased degree of misfit, and hence more load transfer, compared with that at higher loading rates for the same temperature.

Fig. 6 shows the dominant deformation mechanism regimes, as defined in Fig. 4, superimposed on the stress ratio plot. Care needs to be exercised in the interpretation of this plot. The solid line and dashed line adjoining regions IV and V represent boundaries between different classes of behaviour in the conventional sense and were determined by selecting the fastest of a number of competing mechanisms in each phase. The lower dashed boundary was determined, however, by selecting the slowest glide controlled plasticity mechanism. A consequence of this is that the constant strain rate contours do not cross this boundary. As the temperature is increased from 0 K, the stress ratio gradually decreases until the constant strain rate contour touches

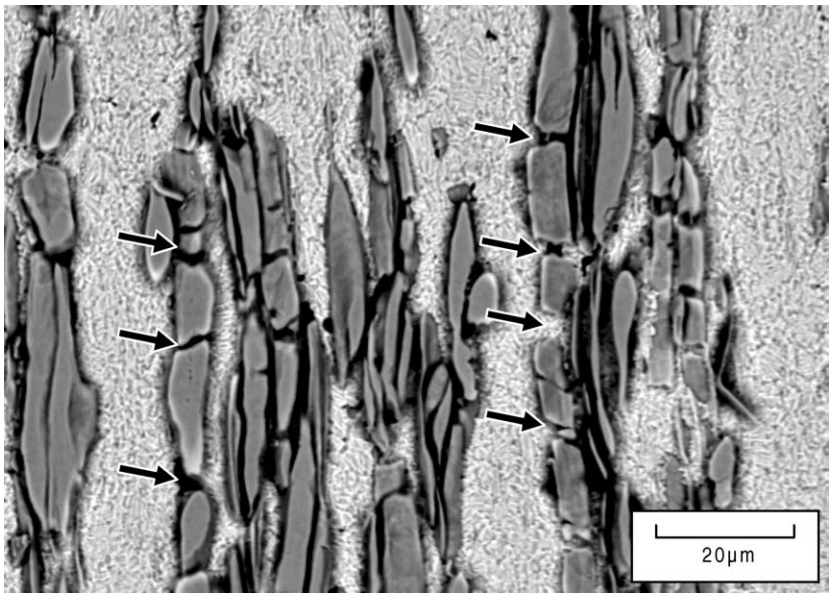

Figure 7 Typical micrograph obtained near the fracture surface of Cu-10 vol% Cr specimen tested at –70°C. Note that damage is in the form of reinforcement cracking (indicated by the arrows).

the lower dashed line of Fig. 6. Up to this point plastic deformation in the Cr is lattice resistance controlled. As the temperature is increased still further, obstacle controlled glide becomes the dominant mechanism in the Cr and the stress ratio increases again. Thus the minima in the stress ratio curves correspond to a change in dominant mechanism from lattice resistance controlled glide to obstacle controlled glide within the Cr phase.

These observations on load transfer have important implications for the expected failure mechanisms of the composite. At low temperatures, load transfer occurs to the Cr, and, since it is brittle because of its high lattice resistance, damage is expected to occur in the form of reinforcement cracking. This has been observed experimentally as shown in Fig. 7. Fibre cracking is severe and frequent at –70°C, suggesting the ductility of Cr fibres decreases rapidly below room temperature. At intermediate temperatures, where there is no significant load transfer, a simple ductile failure should be observed, without any of the damage typically observed in conventional MMCs.

At high temperatures, load transfer will result in significant stresses within the Cr reinforcement. However, unlike the low temperature situation, the Cr is ductile and unlikely to fracture. Damage is therefore expected to occur at the interface between the two phases, in the form of cavitation, particularly at the tips of the reinforcement, where the local stresses will be higher than those calculated here. Experimental findings agree well with the predicted behaviour. The tensile tests performed corresponded to a strain rate of $\sim 10^{-3}$ s^{-1}. The model predicts stress ratios of 1.06 at 23°C and 2.6 at 400°C for this strain rate. This would suggest that microstructural damage due to local stresses would not be expected during the room temperature tests, but would be increasingly likely as the test temperature is increased. Fig. 8 shows typical micrographs taken from specimens of Cu-10 vol% Cr tested at 23 and 400°C,

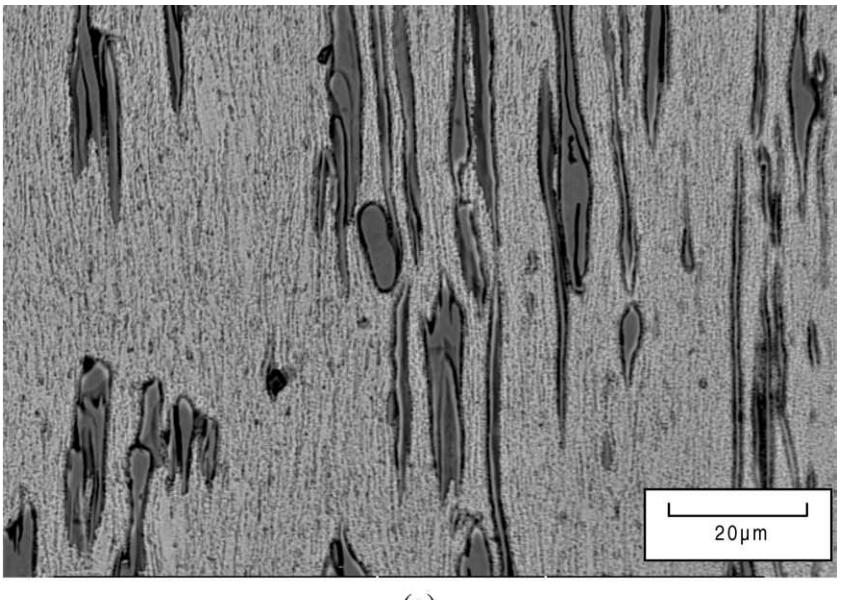

(a)

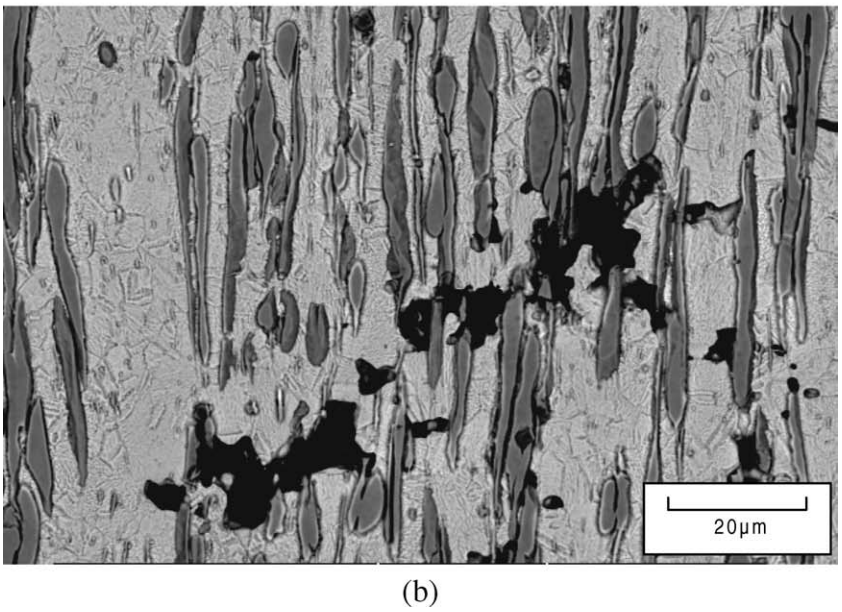

(b)

Figure 8 Typical micrographs obtained near the fracture surface of Cu-10 vol% Cr specimens tested at: (a) 23°C and (b) 400°C. Note that cavitation occurs at high temperatures, but not at room temperature.

near the fracture surface. It can be seen that damage in the form of cavitation only occurs at the higher temperature, which agrees well with the predicted load transfer temperature dependency. There is no significant microstructural damage in the specimen tested at room temperature [15].

4. Conclusions

The concepts of load transfer and misfit between phases have been applied to an *in-situ* Cu-Cr composite to explain the observed mechanical response and failure mechanisms.

A deformation mechanism approach has been used to give information regarding the overall composite deformation rate, and the extent of load transfer within metal/metal composites under different temperature and strain rate conditions. Regimes of dominant deformation mechanism have been identified. Around room temperature the degree of misfit, and hence load transfer to the Cr, during deformation is insignificant. At low temperatures the Cr becomes brittle, leading to behaviour akin to that of conventional composites where the load is transferred to the reinforcement. Significant creep in the Cu at high temperatures results in appreciable misfit and load transfer.

Significant load transfer results in high local stresses which initiate damage processes, such as reinforcement fracture or cavitation. Experimental findings agree well with these predictions.

Acknowledgements

The author is grateful to Chiew Lee, Ying Kuan Liew and Yoong Yoong Lee for their support and encouragement during the duration of this research. Thanks are also due to Claudia Dietz for redrawing Fig. 6.

Appendix

The following equations were utilised in order to obtain the composite deformation mechanism maps. Notation is consistent with that of Frost and Ashby [12].

The strain rate due to discrete obstacle controlled plasticity in each phase, $\dot{\varepsilon}_1$, is given by:

$$\dot{\varepsilon}_1(\sigma, T) = \frac{\gamma_o}{\sqrt{3}} \exp\left[\frac{-\Delta F}{kT}\left(1 - \frac{\sigma}{\sqrt{3}\tau}\right)\right] \quad (2)$$

where γ_o is the pre-exponential and ΔF the activation energy for obstacle controlled glide, k is the Boltzman constant and τ is the obstacle controlled glide flow stress at 0 K.

The strain rate due to lattice resistance limited plasticity in Cr, $\dot{\varepsilon}_2$, is given by:

$$\dot{\varepsilon}_2(\sigma, T) = \frac{\gamma_p}{\sqrt{3}}\left(\frac{\sigma}{\sqrt{3}\mu(T)}\right)^2 \times \exp\left[\frac{-\Delta F_p}{kT}\left[1-\left(\frac{\sigma}{\sqrt{3}\tau_p}\right)^{3/4}\right]^{4/3}\right] \quad (3)$$

where γ_p is the pre-exponential and ΔF_p the activation energy for lattice resistance controlled, μ is the shear modulus and τ_p is the lattice resistance controlled glide flow stress at 0 K.

The strain rate due to power-law creep, $\dot{\varepsilon}_3$, in Cr is given by:

$$\dot{\varepsilon}_3(\sigma, T) = A\left[D_{ov}\exp\left(\frac{Q_v}{RT}\right) + \left(\frac{10a_c D_{oc}}{b^2}\right) \times \left(\frac{\sigma}{\sqrt{3}\mu(T)}\right)^2 \exp\left(\frac{Q_c}{RT}\right)\right]\mu(T)\frac{b}{kT} \times \left(\frac{\sigma}{\mu(T)}\right)^n \quad (4)$$

where A is the Dorn constant for power-law creep, D_{ov} is the pre-exponential and Q_v the activation energy for lattice diffusion, a_c the dislocation core cross section, D_{oc} is the pre-exponential and Q_c the activation energy for dislocation core diffusion, b is the Burger's vector, R is the gas constant and n is the power-law creep exponent.

The strain rate due to power-law creep and power-law breakdown, $\dot{\varepsilon}_4$, in Cu is given by:

$$\dot{\varepsilon}_4(\sigma, T) = \frac{A}{\alpha_p^n}\left[D_{ov}\exp\left(\frac{Q_v}{RT}\right) + 10\left(\frac{a_c D_{oc}}{b^2}\right) \times \left(\frac{\sigma}{\sqrt{3}\mu(T)}\right)^2 \exp\left(\frac{Q_c}{RT}\right)\right] \times \mu(T)\frac{b}{kT}\sinh\left(\frac{\sigma\alpha_p}{\mu(T)}\right)^n \quad (5)$$

where α_p is the reciprocal of the normalised stress at which power-law breakdown occurs.

The strain rate due to diffusional flow in each phase, $\dot{\varepsilon}_5$, is given by:

$$\dot{\varepsilon}_5(\sigma, T) = \frac{14\sigma\Omega}{kTd^2}\left[D_{vo}\exp\left(\frac{-Q_v}{RT}\right) + \frac{\pi}{d}\left(\delta D_{ob}\exp\left(\frac{-Q_b}{RT}\right)\right)\right] \quad (6)$$

where Ω is the atomic volume, δD_{ob} is the boundary diffusion pre-exponential, Q_b is the boundary diffusion activation energy and d is the grain size.

The shear modulus for each phase is given by:

$$\mu(T) = \mu_o\left(1 + \frac{T - 300}{T_m}\mathrm{d}T\right) \quad (7)$$

where μ_o is the modulus at 300 K, T_m is the melting point and $\mathrm{d}T$ is the modulus temperature dependence.

References

1. K. L. LEE, H. E. CARROLL and A. F. WHITEHOUSE, *Mater. Sci. Tech.* **16** (2000) 811.
2. K. L. LEE, A. F. WHITEHOUSE, P. J. WITHERS and M. R. DAYMOND, *Mater. Sci. Eng.* A **348** (2003) 208.

3. K. L. LEE, A. F. WHITEHOUSE, S. I. HONG and A. M. RUSSELL, Accepted for publication in *Metal & Mater Trans* A vol. 35A, p. 695.
4. K. L. LEE, A. F. WHITEHOUSE and A. C. F. COCKS, ICCM 12 Paris (1999).
5. K. L. LEE, *Composites: Part A.* **34**(12) (2003) 1235.
6. S. I. HONG, M. A. HILL, Y. SAKAI, J. T. WOOD and J. D. EMBURY, *Acta Metall. Mater.* **43**(9) (1995) 3313.
7. J. D. VERHOEVEN, W. A. SPITZIG, L. L. JONES, H. L. DOWNING, C. L. TRYBUS, E. D. GIBSON, L. S. CHUMBLEY, L. G. FRITZEMEIER and G. D. SCHNITTGRUND, *J. Mater. Eng.* **12**(2) (1990) 127.
8. T. W. ELLIS, S. T. KIM and J. D. VERHOEVEN, *J. Mater. Engng. Perform.* **4** (1995) 581.
9. C. BISELLI and D. G. MORRIS, *Mater. Sci. Eng.* A **148**(2) (1991) 163.
10. Y. JIN, K. ADACHI, T. TAKEUCHI and H. G. SUZUKI, *ibid.* **212**(1) (1996) 149.
11. *Idem.*, *Metal. Mater. Trans.* A **29**(8) (1998) 2195.
12. H. J. FROST and M. F. ASHBY, "Deformation Mechanism Maps—The Plasticity and Creep of Metals and Ceramics" (Oxford, Pergamon, 1982) p. 161.
13. D. L. ZHANG, K. MIHARA, E. TAKAKURA and H. G. SUZUKI, *Mater. Sci. Eng.* A **266**(1/2) (1999) 99.
14. M. F. ASHBY, *Acta Metall.* **20** (1972) 887.
15. K. L. LEE, A. F. WHITEHOUSE, A. M. RUSSELL, K. WONGPREEDEE, S. I. HONG and P. J. WITHERS, *J. Mater. Sci.* **38** (2003) 3437.
16. K. L. LEE, J. QUINTA DA FONSECA, P. J. WITHERS, S. I. HONG and A. M. RUSSELL, submitted to *Scripta Mater*.

Received 18 June
and accepted 23 December 2003